In *Lectures on Topological Fluid Mechanics* (ed. R.L. Ricca), pp. 179-199.
Lecture Notes in Mathematics, **1973**. Springer-Verlag (2009).

Structural complexity and dynamical systems

Renzo L. Ricca
(School Director and CIME Lecturer)

Abstract With this paper we want to pay tribute to 150 years of work on topological fluid mechanics. For this, we review Helmholtz's (1858) original contribution on topological issues related to vortex motion. Some recent results on aspects of structural complexity analysis of fluid flows are presented and discussed, as well as new results on topological bounds on the energy of magnetic knots and links in ideal magnetohydrodynamics, and on helicity-crossing number relations in dissipative fluids.

1 Introduction

The origin of topological fluid mechanics is probably rooted in the works on vortex motion by Helmholtz (1858) and Lord Kelvin (1869), and much of its modern developments are due to the formidable recent progress in knot theory, vector field analysis, mathematical fluid dynamics and computational visualization. With this paper we want to pay tribute to these 150 years of work on topological fluid mechanics. §1 is dedicated to review Helmholtz's contribution in the light of modern developments in mathematical fluid dynamics: since much of Helmholtz's original emphasis on the relevance of topological issues in fluid mechanics has gradually disappeared from textbooks on vortex dynamics, we simply re-examine his work, emphasizing the merits he deserves for this. §2 overviews some of my recent work on aspects of structural complexity analysis of fluid flows, including a brief summary of some

Renzo L. Ricca
Department of Mathematics and Applications, University of Milano-Bicocca, Via Cozzi 53, 20125 Milano, ITALY.
e-mail: renzo.ricca@unimib.it
http://www.matapp.unimib.it/~ricca/
and
Institute for Scientific Interchange, Villa Gualino, 10133 Torino, ITALY.

current work on applications of critical point theory and topology-based visiometrics. Finally, §3 presents some new results on topological bounds on the energy of magnetic knots and links in ideal magnetohydrodynamics and on helicity-crossing number relations in dissipative fluids.

2 Helmholtz's Work on Vortex Motion: Birth of Topological Fluid Mechanics

It is perhaps little known that the seminal work of Helmholtz (1858; hereafter referred to as H58) *On integrals of the hydrodynamical equations, which express vortex-motion* (Tait's translation) pioneers fundamental questions in topological fluid mechanics. In many ways this is a truly remarkable paper. In addressing and solving the problem of determining rotational motion of fluid elements, for which a single-valued velocity potential cannot be defined, Helmholtz demonstrates three conservation laws for vortex motion (see below), that have become a cornerstone in the foundation of mathematical fluid mechanics (see, for example, Saffman, 1991). The undisputed importance of his main contributions, i.e. the discovery of the conservation laws of vortex motion, has, however, gradually shadowed the strong topological flavour, that permeates the whole paper from the very start. Helmholtz's investigation moves indeed from Euler's original observation of 1755, that even in absence of a kinetic potential certain types of fluid motion are nevertheless possible. In analyzing the conditions of motion, Helmholtz establishes the existence of two classes of hydrodynamic integrals by identifying two separate domains of definition, where either a single-, or a multiple-valued velocity potential is defined, depending on the degree of connection of the fluid region. Conditions for which a single-valued velocity potential exists and the relationship with the multiplicity of connection of the ambient space are discussed in §1 of H58, where it is shown (p. 486) *"that when there is a velocity-potential the elements of the fluid have no rotation, but that there is at least a portion of the fluid elements in rotation when there is no velocity-potential."*

2.1 Multi-Valued Potentials in Multiply Connected Regions

Following Helmholtz's discussion, let us consider an ideal, incompressible fluid in an unbounded, *simply connected* domain $\mathcal{D}$ of $\mathbb{R}^3$. Motion is governed by the standard Euler's equations, supplemented by the incompressibility condition, that is

$$\frac{D\mathbf{u}}{Dt} = -\nabla p + \mathbf{f} \ , \qquad \mathbf{u} = 0 \quad \text{as} \quad \mathbf{X} \to \infty \ , \tag{1}$$

with

$$\nabla \cdot \mathbf{u} = 0 \ , \tag{2}$$

where $\mathbf{u} = \mathbf{u}(\mathbf{X}, t)$ is the velocity of a fluid particle at position $\mathbf{X}$ and time t, p is pressure, $\mathbf{f}$ denotes conservative forces, and fluid density is set to be equal to 1 for convenience. All functions are assumed to be sufficiently smooth at all times. In absence of rotation, we can define a velocity potential ϕ everywhere in $\mathcal{D}$, that is

$$\nabla \times \mathbf{u} = 0 \quad \to \quad \mathbf{u} = \nabla\phi \ ; \tag{3}$$

incompressibility, then, yields the Laplace equation for ϕ, i.e.

$$\nabla \cdot \mathbf{u} = 0 \quad \to \quad \nabla \cdot (\nabla\phi) = \nabla^2\phi = 0 \ , \tag{4}$$

with

$$\phi = \text{cst.} \quad \text{as} \quad \mathbf{X} \to \infty \ , \tag{5}$$

which determines a harmonic, single-valued potential function everywhere in $\mathcal{D}$. Thus, the corresponding integrals of motion are said to be *integrals of the first class* (H58, p. 499). Note that the existence of a single-valued velocity potential ϕ is due to the condition $\nabla \times \mathbf{u} = 0$, everywhere in $\mathcal{D}$. In the language of differential forms this is summarized by the following fundamental relations:

Theorem (Fundamental correspondence). *Let $\mathcal{D}$ be simply connected. Then, we have*

$$\begin{array}{ccc}
\left\{\begin{array}{c} \nabla \times \mathbf{u} = 0 \\ \mathbf{u} \text{ irrotational} \end{array}\right\} & \longleftrightarrow & \left\{\begin{array}{c} \mathrm{d}\alpha = 0 \\ \alpha \text{ closed 1-form} \end{array}\right\} \\
\Updownarrow & & \Updownarrow \\
\mathbf{u} = \nabla\phi & \longleftrightarrow & \alpha = \mathrm{d}\beta \\
\Updownarrow & & \Updownarrow \\
\left\{\begin{array}{c} \mathbf{u} \text{ conservative} \\ \phi \text{ single-valued potential} \end{array}\right\} & \longleftrightarrow & \left\{\begin{array}{c} \alpha \text{ exact} \\ \beta \text{ 0-form} \end{array}\right\} \\
\Updownarrow & & \Updownarrow \\
\int_{\mathcal{C}} \mathbf{u} \cdot \mathrm{d}\mathbf{l} \ , \quad \mathcal{C}\text{-independent} & \longleftrightarrow & \int_{\mathcal{C}} \alpha \ , \quad \mathcal{C}\text{-independent} \\
\Updownarrow & & \Updownarrow \\
\oint_{\mathcal{C}_0} \mathbf{u} \cdot \mathrm{d}\mathbf{l} = 0 \ , \quad \forall \mathcal{C}_0 \text{ in } \mathcal{D} \ . & \longleftrightarrow & \oint_{\mathcal{C}_0} \alpha = 0 \ , \quad \forall \mathcal{C}_0 \text{ in } \mathcal{D} \ .
\end{array}$$

Proof. (Sketch.) Considering first the l.h.s. column, proof of the first top two relations is given by Helmholtz (H58, p. 488–490), while relations at the bottom are consequences of the application of Stokes' theorem. As regards

the r.h.s. column, we can easily see that if α is a closed 1-form, then, by definition, $\mathrm{d}\alpha = 0$ and since $\mathcal{D}$ is simply connected, then it is known the de Rham cohomology group of every closed 1-form on $\mathcal{D}$ is exact (see, for example, Bott & Tu, 1982); hence $\alpha = \mathrm{d}\beta$. On the other hand if α is exact, then, by definition, $\alpha = \mathrm{d}\beta$ and $\mathrm{d}\alpha = \mathrm{d}(\mathrm{d}\beta) = 0$, since every exact differential form is closed. Then, let $\mathcal{C}$ be an oriented smooth 1-manifold in $\mathcal{D}$: α is exact on $\mathcal{C}$ if and only if $\int_{\mathcal{C}} \alpha$ is path-independent on $\mathcal{D}$. Moreover, if $\mathcal{C} = \mathcal{C}_0$ is closed, then, by corollary, $\oint_{\mathcal{C}_0} \alpha$ is path-independent if and only if for every closed 1-manifold in $\mathcal{D}$, $\oint_{\mathcal{C}_0} \alpha = 0$. For the one-to-one correspondences between the two columns see, for example, Weintraub (1997, p. 27 and p. 117).

□

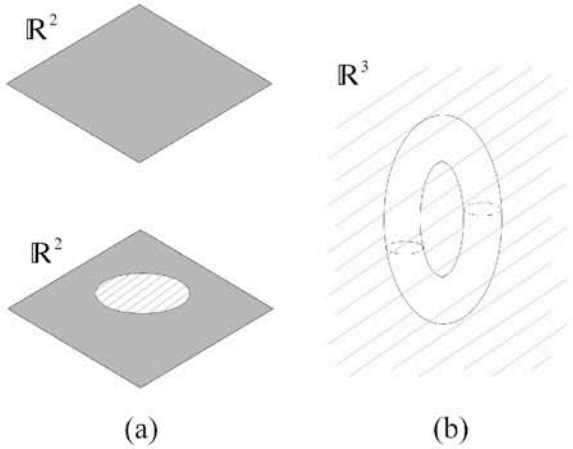

Fig. 1 (a) Simply (top) and doubly connected region in $\mathbb{R}^2$. (b) A vortex ring, defined on a toroidal domain $\mathcal{W} \subset \mathcal{D}$, embedded in an unbounded, irrotational fluid domain, is a doubly-connected region in $\mathbb{R}^3$; note that the complement $\mathcal{D}/\mathcal{W}$, filled by irrotational fluid, is also doubly-connected.

If $\boldsymbol{\omega} = \nabla \times \mathbf{u} \neq 0$ in some region $\mathcal{W} \subset \mathcal{D}$ (and $\nabla \times \mathbf{u} = 0$ everywhere else in $\mathcal{D}/\mathcal{W}$), Helmholtz shows (H58, p. 489–490) that the velocity field $\mathbf{u}$ cannot be given by a single velocity potential ϕ defined in $\mathcal{D}/\mathcal{W}$ through $\nabla\phi$. The presence of a rotational region $\mathcal{W}$, embedded in an unbounded irrotational fluid, makes the irrotational region $\mathcal{D}/\mathcal{W}$ (the complement to $\mathcal{W}$ in $\mathbb{R}^3$) multiply connected. Here Helmholtz refers to the new concepts just developed by Riemann (1857) on multiply connected surfaces. A surface in $\mathbb{R}^2$ is said to be n-ply connected, if there are at most $n-1$ independent, distinct simple circuits, i.e. simple closed paths, irreducible to a point and to one another. The plane in $\mathbb{R}^2$ is an example of simply connected surface (top of Figure 1a), whereas a doubly connected surface has one hole in it

(see bottom of Figure 1a), the latter representing, for example, a region of rotation. Extension of these concepts to $\mathbb{R}^3$ is straightforward (Figure 1b).

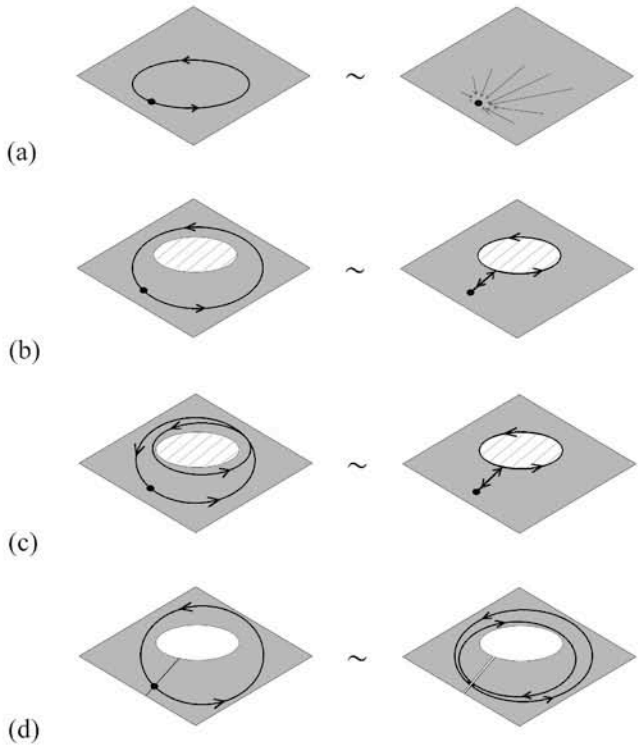

Fig. 2 (a) Every circuit drawn in a simply connected region is reducible to a point, hence the circulation is zero. (b) In a doubly-connected region there is at most one irreducible simple circuit, whose circulation has a finite value, say κ. (c) Example of a multiple circuit ($m = 2$) in a doubly connected region: in this case the circulation is 2κ. (d) A doubly connected region is reduced to a simply connected one by cutting the region with a "circulation-stopping" barrier, represented in figure by the black line.

In a simply connected region every closed path (circuit) is reducible to a point, thus by Stokes' theorem the circulation is zero everywhere (Figure 2a). If the region is doubly connected, though, there is at most one *simple*, irreducible circuit (Figure 2b), whose circulation has a finite value, say κ, which is the *cyclic constant* of the region. The circuit is not simple but *multiple*, if it encircles the rotational region m times, as in Figure 2c; the region's cyclic constant is then $m\kappa$ and in the case of an n-ply connected region the *cyclosis* of the region is given by $\sum_{i=1}^{n-1} m_i\kappa_i$. An n-ply connected region can be reduced to a simply connected one by inserting $n-1$ cuts given by $n-1$ separatrix surfaces drawn across the region (see the case of Figure 2d), each cutting surface diminishing the degree of connectedness by one.

These $n-1$ separatrices act as "stopping barriers" (adopting Lord Kelvin's terminology) to the circulation around the rotational regions, each insertion contributing to the total bounding surface of $\mathcal{D}$. For fluid motions in multiply connected regions the velocity potential takes indeed more than one value. Since the velocity is proportional to the differential coefficients of ϕ, fluid flows are given by ever increasing values of ϕ. But for a fluid particle that moves on a path encircling a rotational region $\mathcal{W}$, as the particle returns to its original position, the potential ϕ attains a second greater value. Hence (H58, p. 499), *"since this may occur indefinitely, there must be for every point of such a complexly-connected space an infinite number of distinct values of ϕ differing by equal quantities like those of* $\tan^{-1}(x/y)$*, which is such a many-valued function and satisfies the differential equation"* given by the second of (4). These observations, applied to fluid dynamics, will be investigated further, and in great depth, by Lord Kelvin (1868, Art. 54 to end), and subsequently elaborated by other authors, including Maxwell (1873, Preliminary, Art. 18–22) and Lamb (1879, Chapter 3, Art. 47–55).

2.2 Green's Theorem in Multiply Connected Regions

Helmholtz (H58, p. 488, footnote) makes another important remark regarding the inapplicability of Green's (first) theorem in presence of rotational motion and multi-valued functions. The standard theorem by Green states that

$$\int_V [\phi\nabla^2\phi' + (\nabla\phi)\cdot(\nabla\phi')]\,\mathrm{dV} = \int_S (\phi\nabla\phi')\cdot\mathrm{d}\mathbf{S}\ , \tag{6}$$

where ϕ and ϕ' denote two velocity potentials, and integration is intended over the volume of the fluid domain and its bounding surface, $\mathrm{d}\mathbf{S}$ denoting an outward-drawn vector element of the surface area. If rotational motion is present in a sub-domain, the region is no longer simply connected and the indeterminacy associated with velocity potentials (assuming that their gradients are single-valued) invalidates the theorem. By taking account of the separatrix surfaces inserted to make the region simply connected, Kelvin (1869) amends the theorem as follows

$$\begin{aligned}&\int_V [\phi\nabla^2\phi' + (\nabla\phi)\cdot(\nabla\phi')]\,\mathrm{dV}\\ &= \int_S (\phi\nabla\phi')\cdot\mathrm{d}\mathbf{S} + \sum_{i=1}^{n-1} m_i\kappa_i \int_{\Sigma_i} \nabla\phi'\cdot\mathrm{d}\boldsymbol{\Sigma}_i\ ,\end{aligned} \tag{7}$$

where integration in the r.h.s. of eq. (7) is now augmented by the sum of the integrals extended to the $n-1$ separatrices of area Σ_i $(i=1,\ldots,n-1)$, each κ_i denoting the jump in ϕ (hence in circulation) across Σ_i. Kelvin's

extension of Green's theorem to multiply connected domains may find useful applications in current theoretical physics: from topological quantum field theory to cosmological models, in presence of black-holes and topological defects.

2.3 Conservation Laws

By considering rotation confined to a tubular-like region (that is a *vortex filament*) embedded in an irrotational fluid, Helmholtz proceeds to prove three laws of conservation for vortex motion. In his own words (H58, §2), he states that:

Theorem (Helmholtz's conservation laws).

1. *Elements of the fluid which at any instant have no rotation, remain during the whole motion without rotation.*
2. *Each vortex line remains continually composed of the same elements of fluid.*
3. *The product of the section and the angular velocity, in a portion of a vortex filament containing the same element of fluid, remains constant during the motion of that element.*

Note the topological character of the first two statements, that can be seen as complement to one another. In modern terms we simply say that a region of vorticity $\mathcal{W}$, embedded in an unbounded, irrotational fluid $\mathcal{D}/\mathcal{W}$, is *frozen* in the fluid and is isotoped to the new region $\varphi_t(\mathcal{W})$ by diffeomorphisms of the flow map φ, by preserving its rotational character at any time; similarly so for the irrotational fluid in the complement region.

3 Measures of Structural Complexity

In recent years the demand for advanced diagnostic tools for computational vortex dynamics, turbulent flows and magnetohydrodynamics has grown considerably (see, for example, Weickert & Hagen, 2006). Detailed analysis of space localization and time evolution of coherent structures, defined by statistical coherence of physically relevant quantities — be these passive scalars, vector or tensor fields — requires new tools to quantify structural complexity present in the fluid (Ricca, 2000; 2001; 2005). Mathematical concepts borrowed from differential geometry, knot theory, graph theory, dynamical systems theory and other branches of modern mathematics can be usefully employed in numerical analysis of direct numerical simulations of fluid flows to quantify, estimate or infer production, transfer and depletion of physical

quantities such as energy and momentum. Current research is mainly oriented in the following directions:

Theoretical goals:
i) to describe and classify complex morphologies;
ii) to study relationships between complexity and energy;
iii) to understand and predict energy localization and transfer.

Applications:
i) to implement new visiometric tools and diagnostics;
ii) to develop real-time energy analysis of dynamical processes;
iii) to compare estimated values with expected values of standard models.

3.1 Dynamical Systems and Vector Field Analysis

A lot of work has been done in this direction, and most notably on the implementation of structural classification of vector fields, on structural stability analysis and on visualization and processing of tensor fields. A very brief summary and a few references are given here for convenience.

Structural classification of vector fields
Structural classification of three-dimensional vector fields $\mathbf{v}(\mathbf{X})$ relies mainly on the eigenvalue/eigenvector analysis of the Jacobian matrix $\mathbf{J}_\mathbf{v}(\mathbf{X}) = \nabla\mathbf{v}(\mathbf{X})$ (see, for example, Chong *et al.*, 1990). A first-order critical point $\mathbf{X}_0$, given by the condition $\mathbf{v}(\mathbf{X}_0) = 0$, can be classified according to the order and value of the real parts of the eigenvalues of $\mathbf{J}_\mathbf{v}(\mathbf{X}_0)$, provided $\det(\mathbf{J}_\mathbf{v}(\mathbf{X}_0)) \neq 0$. Let $\Re e(\lambda_1) \leq \Re e(\lambda_2) \leq \Re e(\lambda_3)$ be the ordered real parts of the eigenvalues; critical points can be classified according to the following scheme:

$$\begin{aligned}
&\text{(i) source :} && 0 < \Re e(\lambda_1) \leq \Re e(\lambda_2) \leq \Re e(\lambda_3)\\
&\text{(ii) repelling saddle :} && \Re e(\lambda_1) < 0 < \Re e(\lambda_2) \leq \Re e(\lambda_3)\\
&\text{(iii) attracting saddle :} && \Re e(\lambda_1) \leq \Re e(\lambda_2) < 0 < \Re e(\lambda_3)\\
&\text{(iv) sink :} && \Re e(\lambda_1) \leq \Re e(\lambda_2) \leq \Re e(\lambda_3) < 0
\end{aligned}$$

where outflow/inflow direction is given by the sign of $\Re e(\lambda_i)$: a negative real part implies inflow (attracting direction) and positive real part implies outflow (repelling direction). Each critical point can be further classified in two families:

$$\begin{aligned}
&\text{(a) focus :} && \Im m(\lambda_i) = 0 \quad \text{and} \quad \Im m(\lambda_j) = -\Im m(\lambda_k) \neq 0\\
&\text{(b) node :} && \Im m(\lambda_i) = \Im m(\lambda_j) = \Im m(\lambda_k) = 0
\end{aligned}$$

where $\Im m(\cdot) =$ denotes imaginary part and $i \neq j \neq k$, $\{i, j, k\} \in \{1, 2, 3\}$, the imaginary part implying circulation. Figure 3 shows an early example of structural classification of streamlines in a three-dimensional separation flow.

Structural stability of dynamical systems
Structural stability issues of dynamical systems rely greatly on the results by Morse, Smale and Peixoto and there is now a wealth of information on divergence-free fields on two-dimensional compact manifolds, motivated by applications to geophysical fluid dynamics. The interested reader may refer to the book by Ma & Wang (2005) for latest results and some generalization to three dimensions.

Visualization and processing of tensor fields
From the early 1990s geometry and topology-driven visualizations have been steadily developed from progress made on structural complexity analysis and critical point theory. These methods are of increasing importance in the analysis and visualization of data-sets from a wide variety of scientific domains. Current challenges include the management of time-dependent data, feature extraction and representation of large and complex data-sets, multi-scale adaptive visualization. The interested reader may consult the collection of papers edited by Hauser *et al.* (2007).

3.2 Measures of Tangle Complexity

Computational fluid dynamics (CFD) produces data-sets of numerical simulations, from which we can extract numerical sub-domains, representing for example vortical or turbulent regions, magnetic field or passive scalar distributions, to analyze. Preliminary steps to any study include: (i) identifying a prescribed sub-domain of physical interest (defined as the *tropicity domain*) and the corresponding characteristic scales, (ii) determining the characteristic dimensions of the chosen region, (iii) assigning a reference system. The physical problem and numerical threshold associated with the CFD code will give information on step (i), while step (ii) and (iii) serve to perform analysis on structural complexity.

Tropicity dimensions and tropicity directions
Let $\mathcal{T} = \bigcup_i \chi_i$ $(i = 1, \ldots, n)$ be the n-component tangle given by the set of vector fields (such as streamlines, vortex lines or magnetic fields) or solution trajectories (e.g. pressure or temperature distributions) to be analyzed. For each tangle component χ_i we can determine the maximal *tropicity dimensions*, given by

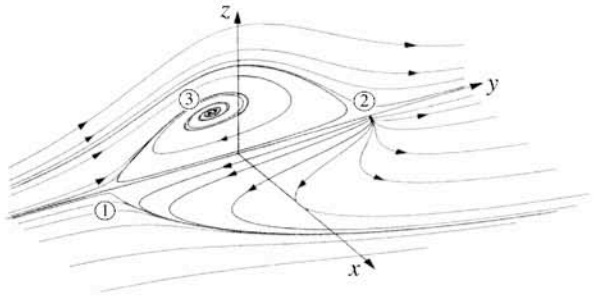

Fig. 3 Study of a three-dimensional separation flow by analysis of the surface streamline pattern (on the $x-y$ plane) and of the solution trajectories (on the plane of symmetry $y-z$). Note that there are 3 major critical points: point 1 is a no-slip saddle, point 2 is a no-slip node in the $x-y$ plane, and point 3 is a free-slip focus in the $y-z$ plane (from Chong *et al.*, 1990).

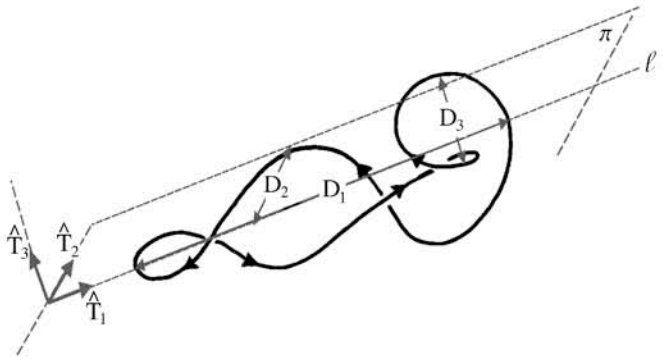

Fig. 4 Tropicity dimensions and reference basis determined by the tangle component χ_i.

$$\left.\begin{aligned} D_1^{(i)} &= \overline{P_0P_1} \equiv \max_{\{j,k\}} d(P_j,P_k)\ , \\ D_2^{(i)} &= \overline{OP_2} \equiv \max_j d(P_j,\ell(P_0,P_1))\ , \\ D_3^{(i)} &= \overline{QP_3} \equiv \max_j d(P_j,\pi(P_0,P_1,P_2))\ , \end{aligned}\right\} \tag{8}$$

where the points P_j, P_k are sampled over χ_i; hence, the principal *tropicity unit vectors* are given by

$$\left.\begin{aligned} \hat{\mathbf{T}}_1^{(i)} &\equiv (P_1-P_0)/D_1^{(i)}\ , \\ \hat{\mathbf{T}}_2^{(i)} &\equiv (P_2-O)/D_2^{(i)}\ , \\ \hat{\mathbf{T}}_3^{(i)} &\equiv \hat{\mathbf{T}}_1^{(i)} \times \hat{\mathbf{T}}_2^{(i)}\ . \end{aligned}\right\} \tag{9}$$

$\{\hat{\mathbf{T}}_1^{(i)}, \hat{\mathbf{T}}_2^{(i)}, \hat{\mathbf{T}}_3^{(i)}\}$ define the reference system on χ_i, (see Figure 4). By averaging this information over n components, we obtain the tropicity dimensions and the reference system of the tangle, that is

$$\left.\begin{aligned} D_1 &= \langle D_1^{(i)} \rangle \ , \qquad \hat{\mathbf{T}}_1 = \langle \hat{\mathbf{T}}_1^{(i)} \rangle \ , \\ D_2 &= \langle D_2^{(i)} \rangle \ , \qquad \hat{\mathbf{T}}_2 = \langle \hat{\mathbf{T}}_2^{(i)} \rangle \ , \\ D_3 &= \langle D_3^{(i)} \rangle \ , \qquad \hat{\mathbf{T}}_3 = \langle \hat{\mathbf{T}}_3^{(i)} \rangle \ , \end{aligned}\right\} \tag{10}$$

Note that the tangle tropicity vectors, are determined by the global geometry of the tangle, and in general do not coincide with the eigenvectors of the Jacobian matrix of the velocity gradients.

Tangle analysis by indented projections
Tropicity directions find applications in tangle analysis. The latter is based on the concept of projected diagrams. Let us consider first a single component χ (for simplicity we shall drop the suffix) and its "indented" projection χ_p, obtained by the orthogonal projection p on the plane of projection Π_p (see Figure 5): by allowing small indentations at crossing sites of the projected curve, the indented projection retains the information associated with over- and under-passes of the original curve viewed along the projection direction. Evidently χ_p depends on the direction of projection, and any change in the latter is obviously reflected in the shape of χ_p. Topological information can be recovered by implementing the three Reidemeister moves computationally, to reduce χ_p to its minimal form, i.e. with minimal number of crossings. By assigning the value $\epsilon_r = \pm 1$ to each apparent crossing of χ_p, according to the sign convention shown in Figure 5, we can compute three important quantities. The first is the *writhing number* Wr, given by

$$Wr_i = Wr(\chi_i) = \langle \sum_{r \in \chi_i} \epsilon_r \rangle \ , \qquad Wr = Wr(\mathcal{T}) = \langle \sum_{r \in \mathcal{T}} \epsilon_r \rangle \ , \tag{11}$$

where here brackets denote averaging over all directions of projection. This quantity gives geometric information on average chirality and associated degree of three-dimensional average coiling in the tangle.

A second important quantity is the total *linking number* $Lk_{\rm tot}$, given by

$$Lk_{ij} = Lk(\chi_i, \chi_j) = \frac{1}{2} \sum_{\substack{r \in \chi_i \sqcap \chi_j \\ i \neq j}} \epsilon_r \ , \qquad Lk_{\rm tot} = \sum_{i \neq j} |Lk_{ij}| \ , \tag{12}$$

where $\sqcap$ denotes disjoint union on the apparent intersections of curve strands, omitting self-crossings. This quantity provides topological information on tangle complexity and changes with the recombination of tangle components.

A third quantity, of algebraic character, that provides a good measure of structural complexity is given by the *average crossing number* $\overline{C}$, defined by

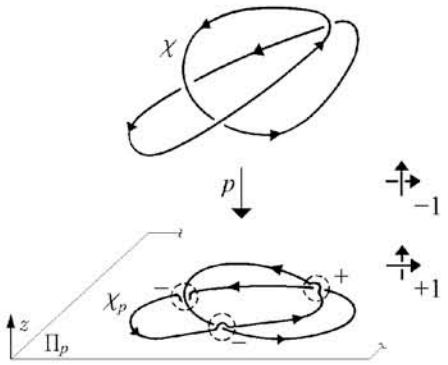

Fig. 5 Indented projection of the tangle component χ under p. The signs at each crossing site of the indented diagram are assigned according to the convention rule shown on the right-hand-side.

the sum of all un-signed crossings, averaged over all projections. We have

$$\overline{C}_{ij} = \overline{C}(\chi_i, \chi_j) = \langle \sum_{r \in \chi_i \# \chi_j} |\epsilon_r| \rangle \ , \qquad \overline{C} = \sum_{r \in \mathcal{T}} \overline{C}_{ij} \ , \tag{13}$$

where # denotes now disjoint union on all apparent intersections of curve strands, including self-crossings.

The average over all directions of projection is either computationally expensive or, in some cases, simply impossible: a more practical approach is to resort to estimated values based, for example, on projections along the tropicity directions $\{\hat{\mathbf{T}}_1, \hat{\mathbf{T}}_2, \hat{\mathbf{T}}_3\}$. The estimated writhing number and the estimated average crossing number are thus given by

$$Wr_\perp = \left(\sum_{r \in \mathcal{T}} \epsilon_r \right)_\perp \ , \qquad \overline{C}_\perp = \left(\sum_{r \in \mathcal{T}} |\epsilon_r| \right)_\perp \ , \tag{14}$$

where $\perp$ denotes the algebraic mean over the three principal projections. Additional information comes also from classical geometric and topological analysis on tangle components (see, for instance, Ricca, 2000).

Comparative analysis on a test case: superfluid vortex tangle
Comparative analysis on the above measures has been conducted by direct numerical simulations of vortex tangles (Barenghi *et al.*, 2001; 2002), produced by perturbations due to a background flow field, or by a decaying turbulent field. Here we report the test case of a superfluid vortex tangle, produced by a background ABC-type of flow. Complexity measures are extracted from the data-sets as the tangle grows in time (see Figure 6) and analysis of growth rates is performed when the tangle is fully developed (between $t = 0.06$ and $t = 0.09$). Physical quantities such as kinetic helicity H,

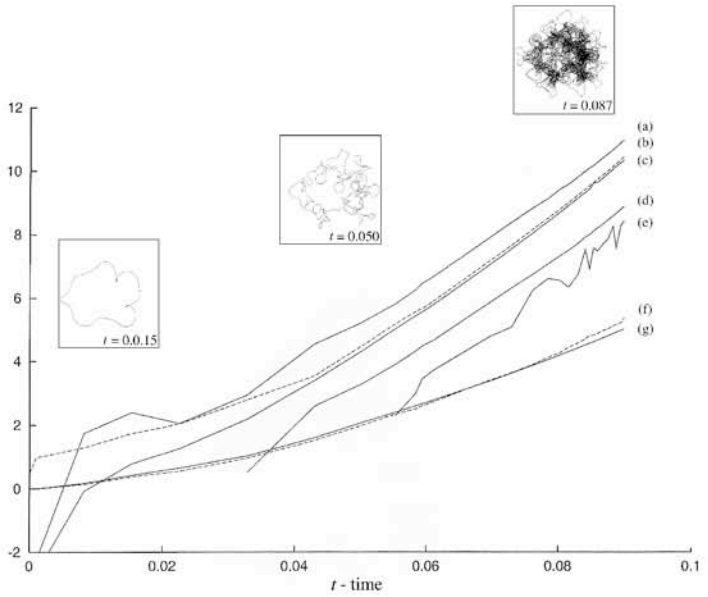

Fig. 6 Comparative analysis of complexity measures for superfluid vortex tangle simulation: tangle mature growth is shown in inset at $t = 0.087$. (a) $\log |H|$; (b) $\log \overline{C}_{\perp}$; (c) $\log \overline{C}$; (d) $\log Wr_{\perp}$; (e) $\log Lk_{\mathrm{tot}}$; (f) $\log(E/E_0)$; (g) $\log(L/L_0)$ (from Barenghi *et al.*, 2001).

normalized kinetic energy E/E_0 and normalized total length L/L_0 are also shown for comparison and check.

The mature stage is characterized by two distinct growth rates: energy/length growth rate $\approx O(83s^{-1})$; complexity measures and helicity growth rate $\approx O(165s^{-1})$. It is remarkable that essentially all the measures tested have similar growth rate. In any case the average crossing number seems to be the most appropriate candidate measure of structural complexity. Comparison between the theoretical value $\overline{C}$, obtained by implementing the analytical definition by Freedman & He (1991) and its estimated value $\overline{C}_{\perp}$, shows that the estimated value — much more convenient computationally — approximates very well the theoretical value. Note also that the discontinuous behaviour of Lk_{tot} is given by topological changes associated with vortex reconnection, but its mean growth rate does not differ significantly from that of other measures.

Tangle analysis by signed area information

If we consider standard projection, instead of indented projection, the projected diagram is a planar nodal curve. In case of thin vortex filaments, as in superfluids, signed area information extracted from the planar graph may be used to estimate linear and angular momentum associated with the vortex tangle. This is based on the interpretation of momenta in terms of projected area and on the application of a geometric method to calculate the signed area

of complex graphs (for details, see Ricca, 2008b). Here we want to illustrate briefly this method.

The oriented graph diagram of a tangle of vortex lines is an oriented nodal curve in $\mathbb{R}^2$, and this often attains considerable complexity, particularly as regards the localization of its self-intersections. A necessary first step is to reduce nodal curves of any complexity to *good* nodal curves, that have (at most) double points. Nodal points are classified according to their degree of multiplicity $\mu(P)$ given by the number of arcs incident at the point of intersection P. If P is a double point, then $\mu(P) = 2$. If P is a point of multiplicity $\mu(P) = n$ $(n > 2)$, we can always reduce its multiplicity by "shaking" the graph diagram (actually its pre-image) near P to get $m = \frac{1}{2}(n^2 - n)$ double points, by virtual perturbations of the incident arcs from their location. Thus, if $h^{(n)}$ is the total number of points of multiplicity n, by applying this shaking technique we can always replace these $h^{(n)}$ points with $h(n) = mh^{(n)}$ $(m \geq 3)$ double points. We say that a graph diagram is a *good projection*, when it has at most double points. Hence, by the shaking technique, we can always reduce highly complex graph diagrams to good nodal curves.

Let $\mathcal{C}$ denote one of such good nodal curves on Π, and let $A(\mathcal{C})$ be the corresponding total area. In order to calculate this area, first we need to define the index $\mathcal{I}_P(\mathcal{C})$ of $\mathcal{C}$ associated with any internal point P. Let $P \notin \mathcal{C}$, $\hat{\mathbf{t}}$ the tangent to $\mathcal{C}$ and $\boldsymbol{\rho}$ the radiant vector with foot at P, that intersects $\mathcal{C}$ transversally. At each intersection point $X \in \boldsymbol{\rho} \cap \mathcal{C}$ assign the algebraic sign $\epsilon(X) = \pm 1$, according to the standard convention given by the right-hand rule, that is $\epsilon(X) = +1$ when the frame $\{\boldsymbol{\rho}, \hat{\mathbf{t}}\}$ is positive (see Figure 7a). If X is a double point, then the intersection is computed with one of the neighbouring pairs of the incident, equi-oriented arcs.

Definition. The *index* $\mathcal{I}_P(\mathcal{C})$ of $\mathcal{C}$ at P is the algebraic intersection number given by

$$\mathcal{I}_P(\mathcal{C}) = \sum_{X \in \boldsymbol{\rho} \cap \mathcal{C}} \epsilon(X). \tag{15}$$

Let us now consider the Z sub-domains $\{\mathcal{R}_j\}_{j=1,\ldots,Z}$ determined by $\mathcal{C} \cap \Pi$ and bounded by $\mathcal{C}$, and let $A(\mathcal{R}_j) > 0$ denote their standard area. Since every point $P \in \mathcal{R}_j$ has the same $\mathcal{I}_P(\mathcal{C})$, we shall call $\mathcal{I}_j$ the index associated with any point $P \in \mathcal{R}_j$ and assign this value to each sub-domain $\mathcal{R}_j$ of $\mathcal{C} \cap \Pi$ (see Figure 7b). The signed area of an oriented graph, a concept that can be traced back to Gauss, is thus given by the following rule.

Rule (Signed area). *The signed area $A(\mathcal{C})$ of an oriented, planar nodal curve $\mathcal{C}$, is given by*

$$A(\mathcal{C}) = \sum_{j=1}^{Z} \mathcal{I}_j A(\mathcal{R}_j) \tag{16}$$

where $A(\mathcal{R}_j) > 0$ is the standard area of $\mathcal{R}_j$.

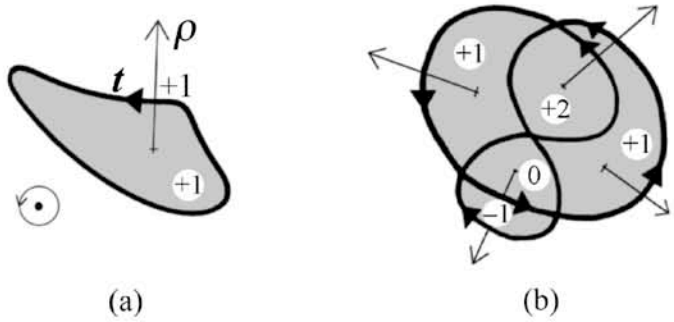

Fig. 7 (a) The number in the dashed region is the value of the index $\mathcal{I}_P(\mathcal{C})$ according to the right-hand rule convention and the algebraic intersection number calculated by eq. (15). (b) The oriented nodal curve, resulting, for example, from the standard projection of a figure-8 knot, has 5 bounded regions. Note that one of the interior regions has index 0, due to the opposite orientation of the strands crossed by $\boldsymbol{\rho}$.

By the signed area rule we can calculate the projected area of any nodal curve, be it the graph of a single vortex line, or that of a complex tangle of vortices. If the vortices have different circulations, a weighting factor defined in terms of contributions from each arc of $\partial\mathcal{R}_j$ must be assigned to $A(\mathcal{R}_j)$. One of the simplest correction comes from an algebraic weighting γ_j of the circulations associated with $\partial\mathcal{R}_j$. Thus, for thin vortices evolving under the so-called localized induction approximation (LIA, for short), we can prove (Ricca, 2008b) the following result:

Theorem (Signed area interpretation). *Let $\mathcal{T}$ be a vortex tangle evolving under LIA. Then, the linear momentum $\mathbf{P} = \mathbf{P}(\mathcal{T})$ has components*

$$P_{xy} = \sum_{j=1}^{Z} \gamma_j \mathcal{I}_j A_{xy}(\mathcal{R}_j), \;\; P_{yz} = \ldots, \;\; P_{zx} = \ldots, \tag{17}$$

and the angular momentum $\mathbf{M} = \mathbf{M}(\mathcal{T})$ has components

$$M_{xy} = d_z \sum_{j=1}^{Z} \gamma_j \mathcal{I}_j A_{xy}(\mathcal{R}_j), \;\; M_{yz} = \ldots, \;\; M_{zx} = \ldots, \tag{18}$$

where $A_{xy}(\mathcal{R}_j)$, ..., etc. denotes standard area of $\mathcal{R}_j$ and d_z distance of the center of mass from the rotational axis.

This method provides a potentially useful tool for predictive and postdictive diagnostics. By analyzing projected areas, it can be applied to implement tests of accuracy of numerical methods simulating vortex tangles. In superfluids, in particular, by analyzing the area distribution of the vortex projection one can judge about the scale distribution of linear and angular momentum, and compare this with the expected values of the spectrum of turbulence

(given, for example, by the Kolmogorov's two-thirds law). Moreover, since LIA preserves an infinity of invariants of motion and *all* of these admit a geometric interpretation in terms of global curvature, torsion and higher order gradients, these can be implemented to supply further information on dynamical properties (for instance, kinetic energy and helicity). Other features associated with the analysis of projected graphs and surface information can be related to dynamical issues: for instance, the Euler characteristic $\chi(G)$ of a graph G associated with a vortex knot or link type. This, being given by $\chi(G) = v - e + r$, where v are the vertices, e the edges and r the regions of G, is a topological invariant related also to the genus $g(F)$ of the Seifert surface F associated with any presentation of the knot or link, by the relation $1 - 2g(F) = \chi(F) = s_0 - c_{\min}$, where s_0 denotes the number of Seifert circles and $c_{\min}$ the topological crossing number of the knot or link. Study of Seifert surfaces of physical systems may reveal interesting properties associated with minimum energy aspects of the system.

4 Topological Bounds on Energy and Helicity-Crossing Number Relations for Magnetic Knots and Links

We restrict our attention to magnetic knots and links: by construction (see, for example, Ricca, 1998) these are tubular embeddings of the magnetic field $\mathbf{B}$ in nested tori T_i $(i = 1, \ldots, n)$ centred on smooth, oriented loops χ_i that are knotted and linked in the fluid domain (see Figure 8). We therefore identify an n-component magnetic link $\mathcal{L}_n$ with the standard embedding of a disjoint union of n magnetic solid tori in $\mathbb{R}^3$:

$$\sqcup_i T_i \hookrightarrow \mathcal{L}_n := \mathrm{supp}(\mathbf{B}) \ . \tag{19}$$

Let $V = V(\mathcal{L}_n)$ be the total volume of the magnetic link.

We take $\mathbf{B} \cdot \boldsymbol{\nu} = 0$ on each tubular boundary ∂T_i of unit normal $\boldsymbol{\nu}$; the flux Φ_i of the magnetic field through each cross-sectional area of T_i is given by:

$$\Phi_i = \int_{T_i} \mathbf{B} \cdot \boldsymbol{\nu} \, \mathrm{d}^2\mathbf{X} \ . \tag{20}$$

Consider the evolution of $\mathcal{L}_n$ under the action of the group of volume– and flux–preserving diffeomorphisms $\varphi : \ \mathcal{L}_n \to \mathcal{L}_{n,\varphi}$. Two fundamental physical quantities of the system are the magnetic energy and the magnetic helicity, respectively defined by:

$$M(t) := \int_{V(\mathcal{L}_n)} \|\mathbf{B}\|^2 \, \mathrm{d}^3\mathbf{X} \ , \qquad H(\mathrm{t}) := \int_{\mathrm{V}(\mathcal{L}_\mathrm{n})} \mathbf{A} \cdot \mathbf{B} \, \mathrm{d}^3\mathbf{X} \ , \tag{21}$$

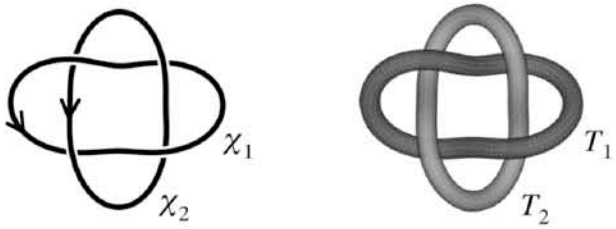

Fig. 8 (a) The 2-component link 4_1^2 with 4 minimum number of crossings is here represented (a) by a disjoint union of 2 oriented loops and (b) by the corresponding centred, tubular neighbourhoods.

where $\mathbf{A}$ is the vector potential associated with $\mathbf{B} = \nabla \times \mathbf{A}$. We take $\nabla \cdot \mathbf{A} = 0$ in $I\!R^3$.

4.1 Topology Bounds Energy in Ideal Fluid

More specifically, let us consider the class of magnetic fields $\mathbf{B} = \mathbf{B}(\mathbf{X}, t)$ that are solenoidal, frozen and of finite energy in an incompressible and perfectly conducting fluid, that is

$$\mathbf{B} \in \{\nabla \cdot \mathbf{B} = 0,\ \partial_t \mathbf{B} = \nabla \times (\mathbf{u} \times \mathbf{B}),\ L_2\text{-norm}\}\ . \tag{22}$$

For frozen fields helicity is a conserved quantity (Woltjer, 1958), thus $H(t) = H =$ constant. It is known that helicity admits topological interpretation in terms of linking numbers (Moffatt, 1969; Berger & Field, 1984; Moffatt & Ricca, 1992):

Theorem. *Let $\mathcal{L}_n$ be an essential magnetic link in an ideal fluid. Then*

$$H = \sum_i Lk_i\, \Phi_i^2 + 2 \sum_{i \neq j} Lk_{ij}\, \Phi_i \Phi_j\ , \tag{23}$$

where Lk_i denotes the Călugăreanu-White linking number of χ_i with respect to the framing induced by the embedding of $\mathbf{B}$ in T_i, and Lk_{ij} denotes the Gauss linking number of χ_i with χ_j.

The Gauss linking number Lk_{ij} is a topological invariant of link types and, admitting interpretation in terms of signed crossings (see first of 12 and Figure 9), it can also be written as

$$Lk_{ij} \equiv \int_{i,j} \mathrm{d}\omega_{\mathrm{i,j}} = \frac{1}{2} \sum_{\substack{\mathrm{r} \in \chi_\mathrm{i} \sqcap \chi_\mathrm{j} \\ \mathrm{i} \neq \mathrm{j}}} \epsilon_\mathrm{r}\ , \tag{24}$$

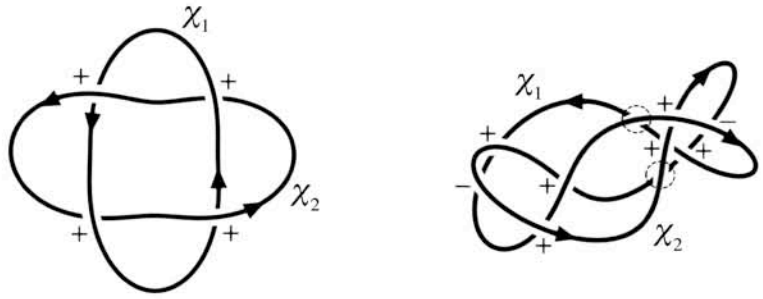

(a) (b)

Fig. 9 (a) The 2-component oriented link 4_1^2 has 4 minimum number of crossings and Gauss linking number $Lk_{12} = 2$. This, being a topological invariant, does not depend on specific projections: the same link type is shown in (a) its minimal projection, with the 4 crossings denoted by the + sign, and in (b) with redundant crossings. Note that the algebraic sum of signed crossings (omitting self-crossings) remains unchanged: the two crossings in (b), denoted by dashed circles, do not contribute to the linking number calculation of eq. (24) because in each case the crossing strands belong to the same link component.

where $\mathrm{d}\omega_{\mathrm{i,j}}$ is the classical Gauss integrand form associated with the two curves χ_i, χ_j and $\sqcap$ denotes apparent intersections of curve strands, omitting self-crossings. The Călugăreanu-White linking number Lk_i is a topological invariant of each link component and admits a geometric decomposition in terms of writhing number Wr_i and twist number Tw_i, according to the well-known formula (Călugăreanu, 1961; White, 1969):

$$Lk_i = Wr_i + Tw_i \ . \tag{25}$$

The writhing number measures the average distortion of χ_i in space, while the total twist measures the total winding of the field lines within T_i.

Assuming for simplicity that all link components have equal flux Φ and be zero-framed, that is $Lk_i = 0$ for all $i = 1, \ldots, n$, lower bounds on energy are given by the following results (for detailed proof see Ricca, 2008a, based on previous works done by Arnold, Freedman & He, and Moffatt):

Theorem. *Let $\mathcal{L}_n$ be an essential magnetic link in an ideal fluid. Then*

$$\text{(i)} \quad M(t) \geq \left(\frac{16}{\pi}\right)^{1/3} \frac{|H|}{V^{1/3}} \ ; \qquad \text{(ii)} \quad M_{\min} = \left(\frac{16}{\pi}\right)^{1/3} \frac{\Phi^2 c_{\min}}{V^{1/3}} \ , \tag{26}$$

where $c_{\min}$ is the topological crossing number of $\mathcal{L}_n$.

The theorem above establishes two important results: (26-i) states that magnetic energy is bounded from below by the absolute value of the helicity (given by the total linking number of the system), scaled by the average size

Fig. 10 Three distinct link types with $n = 2$ and $c_{\min} = 6$. By assuming zero-framing in all link components, same volume V and flux Φ, the three links must have same groundstate energy $M_{\min}$. Thus, different framing should be prescribed if we want to identify uniquely each knot/link type with its specific groundstate energy.

of the system: hence, high helicity concentrations imply greater bounds on energy values. Equality (26-ii) states that the energy minima are actually given by the topological crossing number of the system scaled by the system average size. Note, however, that a classification of knots and links based on energy contents is still incomplete, without prescribing individual framing. By direct inspection of link tabulation, it is indeed immediately evident that there are countably many topologically distinct links with equal number n of (zero-framed) components and same $c_{\min}$ (see Figure 10). This means that a complete classification of magnetic systems by topology is only possible by specifying the individual framing of each component.

4.2 Helicity-Crossing Number Relations in Dissipative Fluid

Suppose now that the fluid is no longer perfectly conducting, but resistive, assuming that the typical dissipation (or reconnection) time scale is higher than the typical evolution time scale so as to preserve magnetic flux. The topology of $\mathcal{L}_n$ may now change due to the effects of dissipation, that make reconnections of the magnetic field lines possible. Under these conditions magnetic helicity may also change, hence $H = H(t)$. Let us define $\Omega := \sum_{\{i,j\}} \mathrm{d}\omega_{\mathrm{i,j}}$; the change in magnetic helicity can be measured in terms of change in algebraic complexity of the magnetic link according to the following result (for proof see Ricca, 2008a).

Theorem. *Let $\mathcal{L}_n$ be a zero-framed, essential magnetic link, embedded in a resistive, incompressible fluid. Then, we have:*

$$\text{(i)} \quad |H(t)| \leq 2\Phi^2 \overline{C}(t) \; ; \quad \text{(ii)} \quad \frac{\mathrm{d|H(t)|}}{\mathrm{dt}} \leq \mathrm{sign}(H)\mathrm{sign}(\Omega) 2\Phi^2 \frac{\mathrm{d}\overline{\mathrm{C}}(\mathrm{t})}{\mathrm{dt}} \; . \quad (27)$$

Direct numerical tests on tangle complexity (cf. results shown in Figure 6; see Barenghi *et al.*, 2001) confirm these results: from the data analysis of the tangle mature growth stage (Φ in appropriate units), we have $[2\overline{C}(0.09) - |H(0.09)|]/|H(0.09)| \approx 19.3\%$ and $\mathrm{sign}(H)\mathrm{sign}(\Omega) = +$, $[2\Delta\overline{C}(t) - \Delta|H(t)|]\Delta|H(t)| \approx 27.6\%$ for $t \in [0.08, 0.09]$. Since these results are independent of specific viscous or resistive time scales, physical time ought to be interpreted in terms of the reconnection time scale involved in the change of topology.

Acknowledgments
Financial support from Italy's MIUR (D.M. 26.01.01, n. 13 "Incentivazione alla mobilità di studiosi stranieri e italiani residenti all'estero") and from ISI-Fondazione CRT (Lagrange Project) is kindly acknowledged.

References

1. Barenghi C.F., Ricca, R.L. & Samuels D.C. (2001) How tangled is a tangle? *Physica* D **157**, 197–206.
2. Barenghi C.F., Ricca, R.L. & Samuels D.C. (2002) Complexity measures of tangled vortex filaments. In *Tubes, Sheets and Singularities in Fluid Dynamics* (ed. K. Bajer & H.K. Moffatt), pp. 69-74. NATO ASI Series, Kluwer.
3. Berger, M.A. & Field, G.B. (1984) The topological properties of magnetic helicity. *J. Fluid Mech.* **147**, 133–148.
4. Bott, R. & Tu, L.W. (1982) *Differential Forms in Algebraic Topology.* Graduate texts in Mathematics **82**, Springer, Berlin.
5. Călugăreanu, G. (1961) Sur les classes d'isotopie des nœuds tridimensionnels et leurs invariants. *Czechoslovak Math. J.* **11**, 588–625.
6. Chong, M.S., Perry, A.E. & Cantwell, B.J. (1990) A general classification of three-dimensional flow fields. *Phys. Fluids* A **2**, 765–777.
7. Freedman, M.H. & He, Z.-X. (1991) Divergence-free fields: energy and asymptotic crossing number. *Ann. Math.* **134**, 189–229.
8. Hauser, H., Hagen, H. & Theisel, H. (2007) (Eds.) *Topology-based Methods in Visualization.* Springer, Berlin.
9. Helmholtz, H. (1858) Über integrale der hydrodynamischen gleichungen welche den wirbelbewegungen entsprechen. *Crelle's J.* **55**, 25–55. [Transalted by P.G. Tait: (1867) On integrals of the hydrodynamical equations, which express vortex motion. *Phil. Mag.* **33**, 485–512.]
10. Lamb, H. (1879) *Treatise on the Mathematical Theory of Motion of Fluids.* Cambridge University Press, Cambridge.
11. Lord Kelvin (Thomson, W.) (1869) On vortex motion. *Trans. Roy. S. Edinburgh* **25**, 217–260.
12. Ma, T. & Wang, S. (2005) *Geometric Theory of Incompressible Flows with Applications to Fluid Dynamics.* Mathematical Surveys and Monographs **119**, American Mathematical Society.
13. Maxwell, J.C. (1873) *A Treatise on Electricity and Magnetism.* Clarendon Press, London.
14. Moffatt, H.K. (1969) The degree of knottedness of tangled vortex lines. *J. Fluid Mech.* **35**, 117–129.

15. Moffatt, H.K. & Ricca, R.L. (1992) Helicity and the Călugăreanu invariant. *Proc. R. Soc.* A **439**, 411–429.
16. Ricca, R.L. (1998) Applications of knot theory in fluid mechanics. In *Knot Theory* (ed. V.F.R. Jones *et al.*), pp. 321-346. Banach Center Publs. **42**, Polish Academy of Sciences, Warsaw.
17. Ricca, R.L. (2000) Towards a complexity measure theory for vortex tangles. In *Knots in Hellas '98* (ed. C. McA. Gordon *et al.*), pp. 361-379. Series on Knots & Everything **24**, World Scientific, Singapore.
18. Ricca, R.L. (2001) Tropicity and complexity measures for vortex tangles. In *Quantized Vortex Dynamics and Superfluid Turbulence* (ed. C.F. Barenghi *et al.*), pp. 366–372. Springer Lecture Notes in Physics **571**, Springer, Berlin.
19. Ricca, R.L. (2005) Structural complexity. In *Encyclopedia of Nonlinear Science* (ed. A. Scott), pp. 885-887. Routledge, New York and London.
20. Ricca, R.L. (2008a) Topology bounds energy of knots and links. *Proc. R. Soc.* A **464**, 293–300.
21. Ricca, R.L. (2008b) Momenta of a vortex tangle by structural complexity analysis. *Physica* D, in press. (doi:10.1016/j.physd.2008.01.002).
22. Riemann, B. (1857) Lehrsätze aus der analysis situs für die theorie der integrale von zweiigliedrigren vollständingen differentialien. *Crelle's J.* **54**, 105–110.
23. Saffman, P.G. (1991) *Vortex Dynamics*. Cambridge University Press, Cambridge.
24. Weickert, J. & Hagen, H. (Eds.) (2006) *Visualization and Processing of Tensor Fields*. Springer, Berlin.
25. Weintraub, S.H. (1997) *Differential Forms*. Academic Press Inc., San Diego.
26. White, J.H. (1969) Self-linking and the Gauss integral in higher dimensions. *Amer. J. Math.* **91**, 693–728.
27. Woltjer, L. (1958) A theorem on force-free magnetic fields. *Proc. Natl. Acad. Sci. USA* **44**, 489–491.